ACS Catalysis

Letter

pubs.acs.org/acscatalysis

High-Efficiency Electrochemical Hydrogen Evolution Catalyzed by Tungsten Phosphide Submicroparticles

Zhicai Xing,[†] Qian Liu,[†] Abdullah M. Asiri,[‡,§] and Xuping Sun*[,†,‡,§]

[†]State Key Laboratory of Electroanalytical Chemistry, Changchun Institute of Applied Chemistry, Chinese Academy of Sciences, Changchun 130022, Jilin China

[‡]Chemistry Department, King Abdulaziz University, Jeddah 21589, Saudi Arabia

[§]Center of Excellence for Advanced Materials Research, King Abdulaziz University, Jeddah 21589, Saudi Arabia

Supporting Information

ABSTRACT: The development of high-efficiency non-noble-metal hydrogen evolution reaction (HER) electrocatalysts operating at all pH values is highly desired but still remains a challenge. In this letter, we report on developing tungsten phosphide submicroparticles as a high-efficiency HER catalyst with high durability for electrochemical hydrogen generation in acidic water. This catalyst shows a low onset overpotential of 54 mV, a Tafel slope of 57 mV/dec, an exchange current density of 0.017 mA/cm^2, and nearly 100% Faradaic efficiency. It needs overpotentials of 115 and 161 mV to afford current densities of 2 and 10 mA/cm^2, respectively. Moreover, this catalyst is also good in activity and durability under neutral and basic conditions.

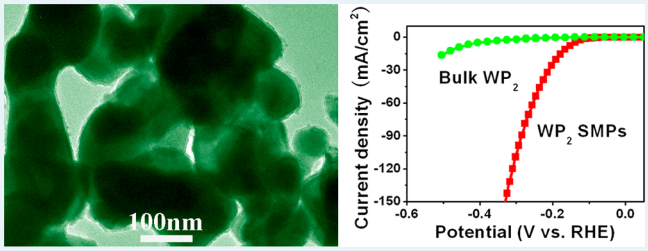

KEYWORDS: *tungsten phosphide, submicroparticles, hydrogen evolution reaction, electrocatalysts, water splitting*

Hydrogen production has attracted great scientific interest because of its relevance to renewable energy storage and its potential for providing energy without the emission of carbon dioxide.[1,2] Electrochemical water splitting, as a simple way for large-scale hydrogen production, needs efficient electrocatalysts for the hydrogen evolution reaction (HER) to afford high current at low overpotential (η).[3] The most active HER catalysts currently known are Pt-group metals, but they are too expensive to be widely used. The strongly acidic conditions involved in proton exchange membrane (PEM) technology require using acid-stable HER catalysts compatible with PEM-based electrolysis units.[4] Abundant nickel-based materials are active for hydrogen evolution;[5,6] however, their poor corrosion stability in acidic media appears to be a significant obstacle to such application. These limitations have led to increased research interest into exploring acid-stable inexpensive alternatives in past years. Mo-based compounds are a big family of such catalysts with great success, including MoS_2, $MoSe_2$, Mo_2C, MoB, $NiMoN_x$, and $Co_{0.6}Mo_{1.4}N_2$,[7−17] among others. In addition, microbial electrolysis cell needs HER catalysts operating under neutral conditions,[18] whereas alkaline water electrolysis requires using catalysts efficiently in basic media.[19] It is thus highly desired to design high-efficiency non-noble-metal HER catalysts capable of operating under all pH conditions; however, to the best of our knowledge, only very limited of such catalysts based on cobalt have been successfully developed so far.[20,21]

W is similar to Mo as they are in the same group, and it has also emerged as an interesting non-noble metal for its catalytic power toward electrochemical hydrogen evolution. Tungsten carbides are active for the HER under acidic conditions, but they suffer from limited corrosion stability, especially at neutral and higher pH values.[22] Although W_2N nanowires exhibit improved stability, they need a large overpotential of 500 mV to afford current density of 10 mA/cm^2.[22,23] Considerable research efforts have been devoted to developing WS_2 catalysts with attractive catalytic activity in acidic media, but these catalysts suffer from intrinsic poor electrical conductivity.[24−29] Transition metal phosphides are interstitial alloys having good electrical conductivity,[30] and this property is a great benefit to electrochemical performance of catalysts. Many recent studies from our laboratory and from other groups have proven the superior HER catalytic performance of transition metal phosphides based on Fe-group and Mo elements.[20,31−42] The electrocatalytic behavior of tungsten phosphide for hydrogen evolution, however, has been paid less attention. Only until recently have amorphous WP nanoparticles been developed as an efficient HER catalyst operating in acidic solutions.[43] In this letter, we report our recent effort toward this direction in developing P-rich tungsten phosphide, WP_2, submicroparticles (WP_2 SMPs) capable of electrochemically catalyzing high-efficiency hydrogen evolution in acidic media. This catalyst requires overpotentials of 115 and 161 mV to achieve current

Received: September 30, 2014
Revised: November 21, 2014
Published: November 21, 2014

densities of 2 and 10 mA/cm^2, respectively, with high durability. It also shows good activity and durability in neutral and basic solutions.

The WP_2 SMPs were prepared through a temperature-programmed hydrogen reduction of air-calcined precursor obtained from $(NH_4)_6{\cdot}H_2W_{12}O_{40}{\cdot}xH_2O$, $(NH_4)_2HPO_4$ and citric acid with mole ratio of 1:2:2. The X-ray diffraction (XRD) pattern for the product only shows peaks characteristic of WP_2 phase (JCPDS No. 35-1467), as shown in Figure 1a. It is

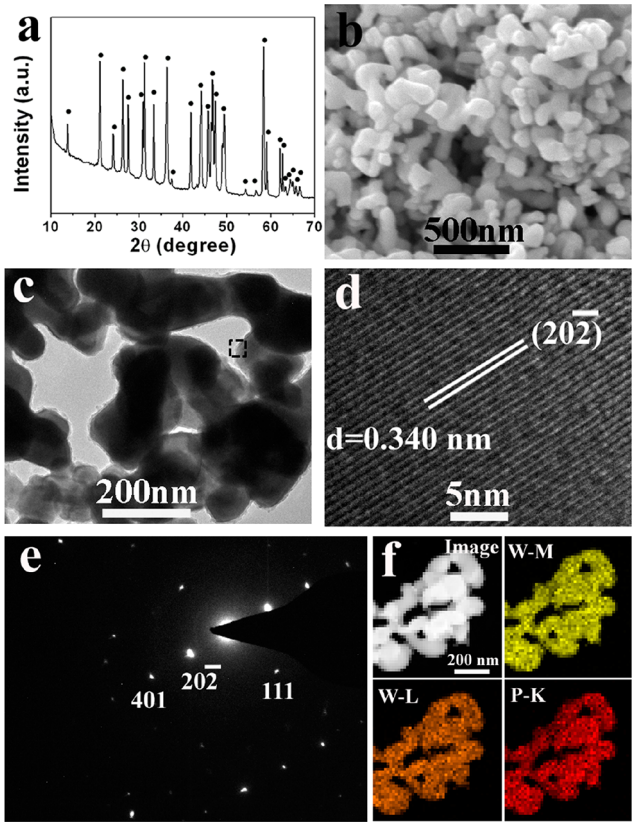

Figure 1. (a) XRD pattern, (b) SEM image, (c) TEM image, (d) HRTEM image, and (e) SAED pattern taken from the area marked with a black rectangle in (c). (f) STEM image and EDX elemental mapping of W and P for the WP_2 SMPs.

reported that WP_2 has MoP_2-type structure, and its crystal structure consists of a molecular channel pair hybridized by both zigzagging layered channel and five ring-pore structures.[44,45] Each W atom is coordinated with seven neighboring P atoms with six P atoms located at the corners of a prism, and the W atom is bonded with a residue P atom located at one of the faces of the prism.[45] Figure S1a and S1b show the X-ray photoelectron spectroscopy (XPS) spectra in the W and P regions for WP_2 SMPs, respectively. Two peaks at 32.1 and 34.2 eV are attributed to W $4f_{7/2}$ and W $4f_{5/2}$, respectively. The high-resolution P(2p) region shows two peaks at 130.8 and 130.0 eV, reflecting the binding energy of P $2p_{1/2}$ and P $2p_{3/2}$, respectively.[46] The predominant P species with binding energy of 130.0 eV is assigned to P bonded to W, while the small peak at 134.1 eV is assigned to oxidized P species arising from surface oxidation due to air contact.[47,48] The survey spectrum (Figure S1c) confirms the existence of oxygen in the sample.

The scanning electron microscopy (SEM) image clearly suggests a large amount of submicroparticles (Figure 1b) were obtained. The energy dispersive X-ray (EDX) spectrum shows a W/P ratio of 32:68, which is consistent within experimental error with the expected 1:2 stoichiometry of WP_2 (Figure S2). The transmission electron microscopy (TEM) image further shows that these submicroparticles are irregular in shape with diameter ranging from 150 to 400 nm (Figure 1c). Although these particles seem to have direct physical contact to form aggregated block, they are well-dispersed in water and thus easily processable, which is a good merit for the preparation of catalysts ink. The high-resolution TEM (HRTEM) image taken from the selected area in Figure 1c reveals clear lattice fringes with an interplane distance of 0.340 nm corresponding to the (20−2) plane of WP_2, as shown in Figure 1d. The corresponding selective area electron diffraction (SAED) pattern of the same area exhibits several bright rings made up of discrete spots, which can be indexed to the (20−2), (111), and (401) planes of WP_2 (Figure 1e). Figure 1f shows the scanning TEM (STEM) image and the corresponding EDX elemental mapping images of W and P for WP_2, indicating both W and P elements are uniformly distributed throughout the WP_2 SMPs. The nitrogen adsorption/desorption isotherm plot shows that WP_2 SMPs have a Brunauer−Emmett−Teller (BET) specific surface area of 37.4 m^2/g (Figure S3). It is importance to mention that the same preparation without using citric acid leads to bulk WP_2 with specific surface area of 7.8 m^2/g, as shown in Figure S4−S6. Note that four-point probe resistivity measurements shows that the resulting WP_2 is highly electrically conductive with a DC conductivity of 55.3 S/cm, implying it has high electronic transfer ability during electrochemical measurements.

To study the electrocatalytic activity of the WP_2 structures, they were deposited on glassy carbon electrode (GCE) with loading of 0.50 mg/cm^2 and evaluated in 0.5 M H_2SO_4 with a scan rate of 2 mV/s. Bare GCE and commercial Pt/C (20 wt % Pt/XC-72) was also tested for comparison. A resistance test was made, and *iR* correction was applied to all electrochemical measurements. Figure 2a shows the polarization curves. Pt/C exhibits expected HER activity with a near zero overpotential while bare GCE shows very poor HER activity. The bulk WP_2 are not significantly active for the HER with an onset overpotential (vs RHE) of 100 mV and only afford current density of 0.48 mA/cm^2 at an overpotential of 200 mV. In sharp contrast, the WP_2 SMPs are highly active for the HER with a low onset overpotential of 54 mV and further negative potential leads to a sharp rise of cathodic current. This catalyst needs overpotentials of 115, 161, and 294 mV to afford current densities of 2, 10, and 100 mA/cm^2, respectively. These overpotentials compare favorably to the behavior of most reported molybdenum, tungsten, and other non-noble metal based HER catalysts in acidic media (Table S1). The superior HER activity for WP_2 SMPs to bulk WP_2 can be attributed to the following two reasons: (1) their much higher specific surface area favors the exposure of more active sites, leading to improved catalytic activity;[8] (2) their much lower charge-transfer impedance (R_{ct}) (13 Ω) than bulk WP_2 (36 Ω) (Figure S7) leads to more facile electrode kinetics.[49] Although bulk materials generally have low electric resistance due to the reduced grain boundary, a less continuous and compact film is formed because of their large size. That is why bulk WP_2 deposited electrode shows a higher R_{ct}.

Figure 2b shows the Tafel plots for WP_2 SMPs, bulk WP_2, and Pt/C catalysts. The linear portions of the Tafel plots are fitted to the Tafel equation ($\eta = b \log j + a$, where j is the

dx.doi.org/10.1021/cs5014943 | ACS Catal. 2015, 5, 145−149

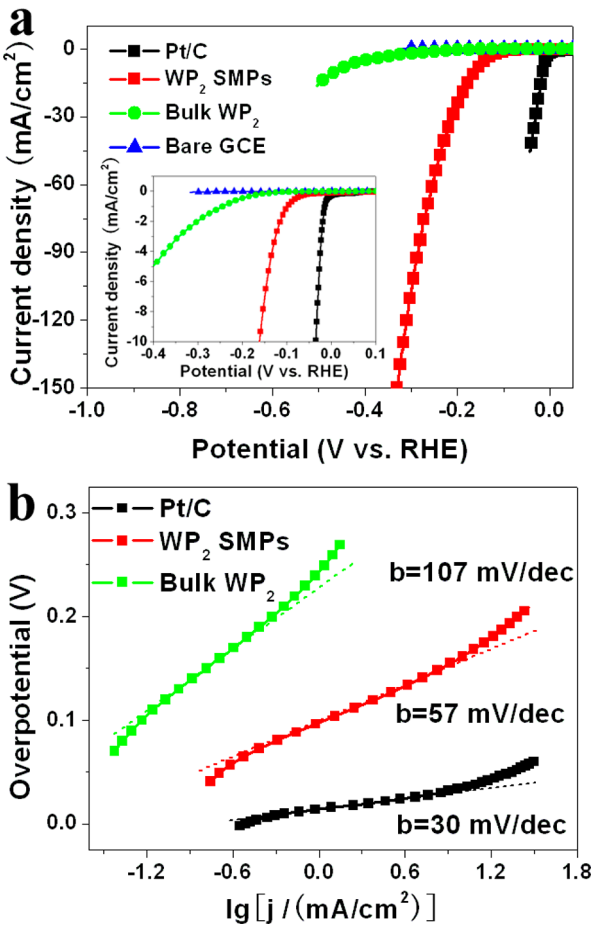

Figure 2. (a) Polarization curves for WP_2 SMPs, bulk WP_2, Pt/C, and bare GCE in 0.5 M H_2SO_4 solution with a scan rate of 2 mV/s. (b) Tafel plots for WP_2 SMPs, bulk WP_2, and Pt/C.

current density and b is the Tafel slope), yielding Tafel slopes of 30, 57, and 107 mV/dec for Pt/C, WP_2 SMPs, and bulk WP_2, respectively. The exchange current density (j_0) of WP_2 SMPs (~0.017 mA/cm^2) is 3 times of that of bulk WP_2 (~0.006 mA/cm^2) (Figure S8). It suggests that the value for WP_2 SMPs is higher than those of bulk WP_2 and most reported non-noble-metal HER catalysts listed in Table S1. The electrochemical active surface area (EASA) for WP_2 SMPs and bulk WP_2 deposited electrodes was estimated to be 4.65 and 1.12 cm^2, respectively (Figure S9). Figure S10 shows the reploted Tafel plots with current normalized by EASA and the Tafel slopes for WP_2 SMPs and bulk WP_2 are 65 and 122 mV/dec, respectively. The EASA normalized j_0 for WP_2 SMPs is 9.12×10^{-4} mA/cm^2, which is about 4 times of that for bulk WP_2 (2.34×10^{-4} mA/cm^2). Given that the BET surface area for WP_2 SMPs is also about 4 times of that for bulk WP_2, we can conclude that both submicroparticles and bulk sample possess similar intrinsic HER activity. The smaller Tafel slope for WP_2 SMPs is possibly a result of the lower R_{ct} for WP_2 SMPs deposited electrode and the HER occurring on a porous matrix with higher specific surface area.[50,51]

Durability was further examined by cycling the WP_2 SMPs modified GCE continuously for 5000 cycles ranging from +0.10 to −0.30 V versus RHE at a scan rate of 100 mV/s. At the end of the cycling procedure, this catalyst shows similar linear sweep voltammetry (LSV) curve to the initial one with negligible loss in current density (Figure 3). The long-term

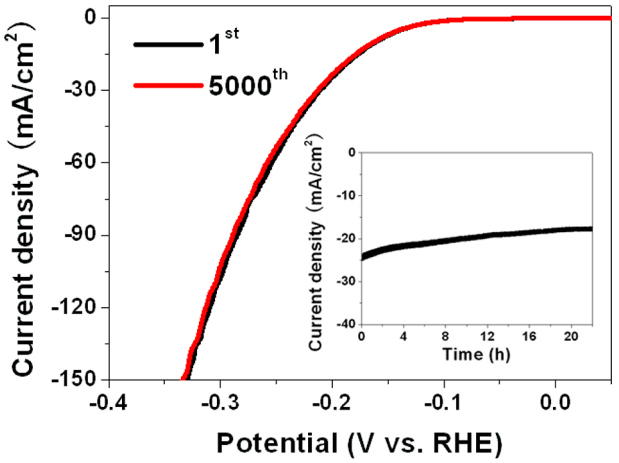

Figure 3. Stability of WP_2 SMPs with an initial polarization curve and after 5000 cycles at a scan rate of 100 mV/s between +0.10 and −0.30 V in 0.5 M H_2SO_4 (inset: time-dependent catalytic current density curve during electrolysis for WP_2 SMPs at η = 200 mV in 0.5 M H_2SO_4).

stability of WP_2 SMPs was also evaluated by electrolysis at a fixed overpotential of 200 mV. Figure 3 inset shows that this catalyst can remain catalytic current density of 20 mA/cm^2 over 22 h. Although this catalyst shows about 20% loss in activity, it still exhibits superior stability in a long-term electrochemical process over some previously reported catalysts like defect-rich MoS_2 nanosheets,[10] FeP arrays,[34,35] Ni_2P Nanoparticles,[39] amorphous MoS_2,[52,53] and so forth.

We further investigated the HER performance of the WP_2 SMPs in 1.0 M PBS (pH 7). It shows an onset overpotential of 60 mV and a Tafel slope of 92 mV/dec with excellent durability (Figure S11a and S11b). This catalyst needs an overpotential of 143 mV to afford current density of 2 mA/cm^2. This overpotential compares favorably to the behavior of most reported Pt-free HER catalysts in neutral media (Table S2). In addition, the WP_2 SMPs are also excellent in activity and durability with a Tafel slope of 60 mV/dec under alkaline condition (Figure S11c and S11d). Overpotentials of 85 and 153 mV are needed for WP_2 SMPs to afford current densities of 1 and 10 mA/cm^2, respectively. These overpotentials are much lower than those used by other non-noble-metal HER catalysts in basic media except Ni−Mo alloy/Ti foil (Table S3). We also determined the Faradaic efficiency of this catalyst for hydrogen evolution using a previously reported method.[20,31−34] The agreement of the amount of experimentally quantified hydrogen with theoretically calculated hydrogen (assuming 100% Faradaic efficiency) suggests that the Faradaic efficiency is close to 100% (Figure S12).

Both hydrogenases[54] and metal complex HER catalysts[55−57] incorporate proton relays from pendant acid−base groups close to the metal center where hydrogen evolution occurs. In our case, the binding energy of W in WP_2 is higher than that of metallic W (31.5 eV), while the BE of P is lower than that of elemental P (130.2 eV),[58] indicating W and P in WP_2 have a partial positive (δ^+) and negative (δ^-) charge, respectively (Figure S1a and S1b), resulting from a small transfer of electron density from W to P in WP_2.[59] Thus, like previously reported HER catalysts based on hydrogenases,[54] metal complexes[55−57] and other transition metal phosphides including CoP,[20,31,32] Cu_3P,[33] FeP,[34,35] Ni_2P,[36] NiP_2[37] and MoP,[38] the WP_2 also features the pendant base P close proximity to the metal center

dx.doi.org/10.1021/cs5014943 | ACS Catal. 2015, 5, 145−149

W, implying both W center and the pendant base P are the active sites for the hydrogen evolution. We may conclude that the W and P act as the hydride acceptor and proton acceptor center, respectively, facilitating the HER,[39,60] and P could also facilitate the formation of W-hydride for subsequent hydrogen evolution via electrochemical desorption.[61]

In conclusion, WP_2 submicroparticles were developed as an efficient hydrogen evolution electrocatalyst in strongly acidic and basic as well as neutral electrolytes. Their electrocatalytic performance places them among the best earth-abundant alternatives to Pt catalyst toward electrochemical water splitting for large-scale hydrogen fuel production. We should mention here that Nafion was used as a polymer binder to effectively immobilize these catalysts on current collectors. Such polymer binder, however, generally increases the series resistance[62] and may block active sites and inhibit diffusion,[63] leading to reduced catalytic activity. Future work will focus on directly growing the active phases on current collectors as binder-free self-supported hydrogen evolution cathodes.

■ ASSOCIATED CONTENT

Supporting Information

The following file is available free of charge on the ACS Publications website at DOI: 10.1021/cs5014943.

Experimental section; XPS and EDS spectra; Nitrogen adsorption/desorption isotherms; SEM images; XRD pattern; Tables S1−S3; Nyquist plots; exchange current calculation; cyclic voltammograms; the EASA normalized polarization curves and Tafel Plots; polarization curves; Tafel plots; Faradaic efficiency determination (PDF)

■ AUTHOR INFORMATION

Corresponding Author

*E-mail: sunxp@ciac.ac.cn (X.S.).

Notes

The authors declare no competing financial interest.

■ ACKNOWLEDGMENTS

This work was supported by the National Natural Science Foundation of China (No. 21175129) and the National Basic Research Program of China (No.2011CB935800).

■ REFERENCES

(1) Dresselhaus, M. S.; Thomas, I. L. *Nature* **2001**, *414*, 33−34.
(2) Lewis, N. S.; Nocera, D. G. *Proc. Natl. Acad. Sci. U.S.A* **2006**, *103*, 15729−15735.
(3) Walter, M. G.; Warren, E. L.; McKone, J. R.; Boettcher, S. W.; Mi, Q.; Santori, E. A.; Lewis, N. S. *Chem. Rev.* **2010**, *110*, 6446−6473.
(4) Le, G. A.; Artero, V.; Jousselme, B.; Tran, P. D.; Guillet, N.; Métayé, R.; Fihri, A.; Palacin, S.; Fontecave, M. *Science* **2009**, *326*, 1384−1387.
(5) Brown, D. E.; Mahmood, M. N.; Man, M. C. M.; Turner, A. K. *Electrochim. Acta* **1984**, *29*, 1551−1556.
(6) Raj, I. A.; Vasu, K. I. *J. Appl. Electrochem.* **1990**, *20*, 32−38.
(7) Jaramillo, T. F.; Jørgensen, K. P.; Bonde, J.; Nielsen, J. H.; Horch, S.; Chorkendorff, I. *Science* **2007**, *317*, 100−102.
(8) Kibsgaard, J.; Chen, Z.; Reinecke, B. N.; Jaramillo, T. F. *Nat. Mater.* **2012**, *11*, 963−969.
(9) Lukowski, M. A.; Daniel, A. S.; Meng, F.; Forticaux, A.; Li, L.; Jin, S. *J. Am. Chem. Soc.* **2013**, *135*, 10274−10277.
(10) Xie, J.; Zhang, H.; Li, S.; Wang, R.; Sun, X.; Zhou, M.; Zhou, J.; Lou, X.; Xie, Y. *Adv. Mater.* **2013**, *25*, 5807−5813.
(11) Li, Y.; Wang, H.; Xie, L.; Liang, Y.; Hong, G.; Dai, H. *J. Am. Chem. Soc.* **2011**, *133*, 7296−7299.
(12) Kong, D.; Wang, H.; Cha, J.; Pasta, M.; Koski, K. J.; Yao, J.; Cui, Y. *Nano Lett.* **2013**, *13*, 1341−1347.
(13) Wan, C.; Regmi, Y. N.; Leonard, B. M. *Angew. Chem., Int. Ed.* **2014**, *53*, 6407−6411.
(14) Cui, W.; Cheng, N.; Liu, Q.; Ge, C.; Asiri, A. M.; Sun, X. *ACS Catal.* **2014**, *4*, 2658−2661.
(15) Vrubel, H.; Hu, X. *Angew. Chem., Int. Ed.* **2012**, *54*, 12703−12706.
(16) Chen, W.; Sasaki, K.; Ma, C.; Frenkel, A. I.; Marinkovic, N.; Muckerman, J. T.; Zhu, Y.; Adzic, R. R. *Angew. Chem., Int. Ed.* **2012**, *51*, 6131−6135.
(17) Cao, B.; Veith, G. M.; Neuefeind, J. C.; Adzic, R. R.; Khalifah, P. G. *J. Am. Chem. Soc.* **2013**, *135*, 19186−19192.
(18) Kundu, A.; Sahu, J. N.; Redzwan, G.; Hashim, M. A. *Int. J. Hydrogen Energy* **2013**, *38*, 1745−1757.
(19) Leroy, R. L. *Int. J. Hydrogen Energy* **1983**, *8*, 401−417.
(20) Tian, J.; Liu, Q.; Asiri, A. M.; Sun, X. *J. Am. Chem. Soc.* **2014**, *136*, 7587−7590.
(21) Zou, X.; Huang, X.; Goswami, A.; Silva, R.; Sathe, B. R.; Mikmeková, E.; Asefa, T. *Angew. Chem., Int. Ed.* **2014**, *53*, 4372−4376.
(22) Chen, W.; Muckerman, J. T.; Fujita, E. *Chem. Commun.* **2013**, *49*, 8896−8909.
(23) Chakrapani, V.; Thangala, J.; Sunkara, M. K. *Int. J. Hydrogen Energy* **2009**, *34*, 9050−9059.
(24) Voiry, D.; Yamaguchi, H.; Li, J.; Silva, R.; Alves, D. C. B.; Fujita, T.; Chen, M.; Asefa, T.; Shenoy, V. B.; Eda, G.; Chhowalla, M. *Nat. Mater.* **2013**, *12*, 850−855.
(25) Yang, J.; Voiry, D.; Ahn, S. J.; Kang, D.; Kim, A. Y.; Chhowalla, M.; Shin, H. S. *Angew. Chem., Int. Ed.* **2013**, *52*, 13751−13754.
(26) Zhao, Y.; Kamiya, K.; Hashimoto, K.; Nakanishi, S. *Angew. Chem., Int. Ed.* **2013**, *125*, 13883−13886.
(27) Lin, J.; Peng, Z.; Wang, G.; Zakhidov, D.; Larios, E.; Yacaman, M. J.; Tour, J. M. *Adv. Energy Mater.* **2014**, DOI: 10.1002/aenm.201301875.
(28) Cheng, L.; Huang, W.; Gong, Q.; Liu, C.; Liu, Z.; Li, Y.; Dai, H. *Angew. Chem., Int. Ed.* **2014**, *53*, 7860−7863.
(29) Lukowski, M. A.; Daniel, A. S.; English, C. R.; Meng, F.; Forticaux, A.; Hamers, R.; Jin, S. *Energy Environ. Sci.* **2014**, *7*, 2608−2613.
(30) Oyama, S. T.; Gott, T.; Zhao, H.; Lee, Y. K. *Catal. Today* **2009**, *143*, 94−107.
(31) Liu, Q.; Tian, J.; Cui, W.; Jiang, P.; Cheng, N.; Asiri, A. M.; Sun, X. *Angew. Chem., Int. Ed.* **2014**, *53*, 6710−6714.
(32) Pu, Z.; Liu, Q.; Jiang, P.; Asiri, A. M.; Obaid, A. Y.; Sun, X. *Chem. Mater.* **2014**, *26*, 4326−4329.
(33) Tian, J.; Liu, Q.; Cheng, N.; Asiri, A. M.; Sun, X. *Angew. Chem., Int. Ed.* **2014**, *53*, 9577−9581.
(34) Jiang, P.; Liu, Q.; Liang, Y.; Tian, J.; Asiri, A. M.; Sun, X. *Angew. Chem., Int. Ed.* **2014**, *53*, 12855−12859.
(35) Liang, Y.; Liu, Q.; Asiri, A. M.; Sun, X.; Luo, Y. *ACS Catal.* **2014**, *4*, 4065−4069.
(36) Pu, Z.; Liu, Q.; Tang, C.; Asiri, A. M.; Sun, X. *Nanoscale* **2014**, *6*, 11031−11034.
(37) Jiang, P.; Liu, Q.; Sun, X. *Nanoscale* **2014**, *6*, 13440−13445.
(38) Xing, Z.; Liu, Q.; Asiri, A. M.; Sun, X. *Adv. Mater.* **2014**, *26*, 5702−5707.
(39) Popczun, E. J.; McKone, J. R.; Read, C. G.; Biacchi, A. J.; Wiltrout, A. M.; Lewis, N. S.; Schaak, R. E. *J. Am. Chem. Soc.* **2013**, *135*, 9267−9270.
(40) Popczun, E. J.; Read, C. G.; Roske, C. W.; Lewis, S.; Schaak, R. E. *Angew. Chem., Int. Ed.* **2014**, *53*, 5427−5430.
(41) Xiao, P.; Sk, M. A.; Thia, L.; Ge, X.; Lim, R. J.; Wang, J.; Lim, K. H.; Wang, X. *Energy Environ. Sci.* **2014**, *7*, 2624−2629.
(42) Xu, Y.; Wu, R.; Zhang, J.; Shi, Y.; Zhang, B. *Chem. Commun.* **2013**, *49*, 6656−6658.
(43) McEnaneya, J. M.; Cromptonb, J. C.; Callejasa, J. F.; Popczuna, E. J.; Reada, C. G.; Lewis, N. S.; Schaak, R. E. *Chem. Commun.* **2014**, *50*, 11026−11028.

(44) Rundqvist, S.; Lundstrom, T. *Acta Chem. Scand.* **1963**, *17*, 37−46.
(45) Kim, M. G.; Lee, S.; Cho. *J. Electrochem. Soc.* **2009**, *156*, A89−A94.
(46) Grosvenor, A. P.; Wik, S. D.; Cavell, R. G.; Mar, A. *Inorg. Chem.* **2005**, *44*, 8988−8998.
(47) Bai, J.; Li, X.; Wang, A.; Prins, R.; Wang, Y. *J. Catal.* **2012**, *287*, 161−169.
(48) Phillips, D. C.; Sawhill, S. J.; Self, R.; Bussell, M. E. *J. Catal.* **2002**, *207*, 266−273.
(49) Guo, C.; Zhang, L.; Miao, J.; Zhang, J.; Li, C. M. *Adv. Energy Mater.* **2013**, *3*, 167−171.
(50) Conway, B. E.; Tilak, B. V. *Electrochim. Acta* **2002**, *47*, 3571−3594.
(51) Lu, Z.; Zhang, H.; Zhu, W.; Yu, X.; Kuang, Y.; Chang, Z. *Chem. Commun.* **2013**, *49*, 7516−7518.
(52) Benck, J. D.; Chen, Z.; Kuritzky, L. Y.; Forman, A. J.; Jaramillo, T. F. *ACS Catal.* **2012**, *2*, 1916−1923.
(53) Laursen, A. B.; Vesborg, P. C. K.; Chorkendorff, I. *Chem. Commun.* **2013**, *49*, 4965−4967.
(54) Nicolet, Y.; de Lacey, A. L.; Vérnede, X.; Fernandez, V. M.; Hatchikian, E. C.; Fontecilla-Camps, J. C. *J. Am. Chem. Soc.* **2001**, *123*, 1596−1601.
(55) Wilson, A. D.; Newell, R. H.; McNevin, M. J.; Muckerman, J. T.; Dubois, M. R.; Dubois, D. L. *J. Am. Chem. Soc.* **2006**, *128*, 358−366.
(56) Wilson, A. D.; Shoemaker, R. K.; Miedaner, A.; Muckerman, J. T.; Dubois, D. L.; Dubois, M. R. *Proc. Natl. Acad. Sci. U.S.A.* **2007**, *104*, 6951−6956.
(57) Barton, B. E.; Rauchfuss, T. B. *J. Am. Chem. Soc.* **2010**, *132*, 14877−14885.
(58) *Practical Surface Analysis by Auger and X-ray Photoelectron Spectroscopy*Briggs, D., Seah, M. P., Eds.; Wiley: New York, 1983.
(59) King, R. B. *Encyclopedia of Inorganic Chemistry*, 2nd ed.; Wiley, Hoboken, NJ, 2005.
(60) Liu, P.; Rodriguez, J. A. *J. Am. Chem. Soc.* **2005**, *127*, 14871−14878.
(61) Zhang, W.; Hong, J.; Zheng, J.; Huang, Z.; Zhou, J.; Xu, R. *J. Am. Chem. Soc.* **2011**, *133*, 20680−20688.
(62) Luo, Y.; Jiang, J.; Zhou, W.; Yang, H.; Luo, J.; Qi, X.; Zhang, H.; Denis, Y.; Li, C. M.; Yu, T. *J. Mater. Chem.* **2012**, *22*, 8634−8640.
(63) Roy-Mayhew, J. D.; Boschloo, G.; Hagfeldt, A.; Aksay, I. A. *ACS Appl. Mater. Interfaces* **2012**, *4*, 2794−2800.